Spectroscopic and Computational Study of $ZnCl_2$–Methanol Low-Melting-Temperature Mixtures

Payam Kalhor, Zhaoxi Sun, and Zhiwu Yu*

ABSTRACT: Alcoholic electrolyte mixtures have wide applica-tions in industries. In this study, a series of mixtures composed of $ZnCl_2$ and methanol (MeOH) with $ZnCl_2$ mol % from 6.7 to 25 were prepared, and their spectral, structural, and thermodynamic properties were studied using infrared (IR) spectroscopy, differential scanning calorimetry (DSC), and density functional theory (DFT) calculations. The DFT-assisted analysis of excess spectra, supported by 2D-correlation spectroscopy, led to the identification of the major constituents of $ZnCl_2$–MeOH mixtures, namely, MeOH monomer, MeOH dimer, and $ZnCl_2$–3MeOH complex, produced after dissociation of MeOH trimer which represents the bulk methanol. The Hirshfeld charge analysis showed that in the competition between the O–H···Cl hydrogen bond (H-bond) and Zn ← O coordination bond to transfer charge in $ZnCl_2$–MeOH complexes, the latter always dominates, making MeOH positively charged. The phase diagram of the binary system showed the presence of V-shaped glass transition temperatures (T_g), characteristic of low-melting mixture solvents (LoMMSs). The present study provides insights into the microscopic properties of the system and sheds light on the understanding of the general principles to prepare deep-eutectic solvents (DESs) or LoMMSs using inorganic salts and alcoholic compounds.

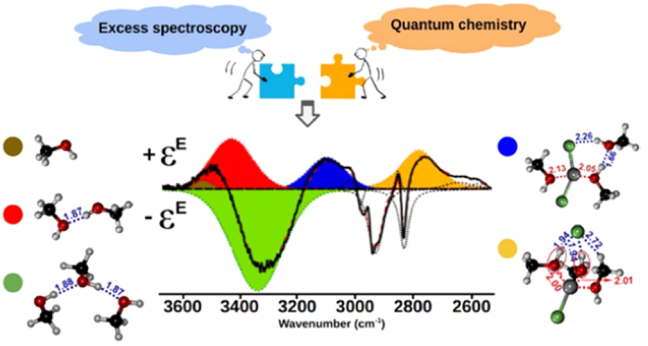

INTRODUCTION

The omnipresence of electrolyte solutions in the natural world has made knowledge of their microscopic and macroscopic properties highly crucial.[1] These properties are significantly altered compared with those of pure components.[1−6] But they are essential to the understanding of the associated chemical and biological processes and the design of novel systems for industrial applications.

Among the electrolyte solutions, the (aqueous) alcoholic electrolyte solutions have been vastly studied with the majority of the efforts made to measure their physicochemical properties.[2−11] In this regard, studying the thermal behavior of such mixtures containing organic or inorganic salts and measuring their phase transitions such as freezing points have been the focus of some studies.[10−14] Among such systems are mixtures with depressed freezing points when compared with those of the pure constituents.[12] These mixtures have been regarded as deep-eutectic solvents (DESs),[15] although their compositions are largely not justified with the eutectic requirements. Very often, the freezing points of the mixtures are absent, and only low-temperature glass transitions (T_g) are observed. For these systems, the term low-transition-temperature mixtures (LTTMs) was suggested to replace DESs.[16,17] Recently, Chen and Yu reviewed these terms critically and proposed using low-melting mixture solvents (LoMMSs) to describe the liquid mixtures when their melting temperatures are lower than those of the individual constituents, regardless of the compositions and the nature of the melting. With this, the concept of DESs is a subset of the concept of LoMMSs.[18] DESs/LoMMSs are usually prepared by simply mixing the starting components at moderate temperatures with at least one of the constituents having a high melting point.[19,20]

There are some reported alcoholic electrolyte solutions which have been found or predicted to form DESs/LoMMSs, such as $ZnCl_2$–ethanol (EtOH),[21] $ZnCl_2$–ethylene glycol (EG),[12] $ZnCl_2$–hexanediol,[12] choline chloride (ChCl)–methanol (MeOH),[22] ChCl–EG,[23] ChCl–glycerol,[23] ChCl–butanediol,[24] ChCl–hexanediol,[24] and betaine hydrochloride–glycerol.[25] Microscopic information on such solutions, however, is largely unknown. Such information not only provides clear pictures of the microscopic nature of the systems but also facilitates the prediction or rationalization of their macroscopic properties. This challenge is mainly posed by the complex nature of the electrolyte solutions with short-range

repulsive and long-range attractive interactions associated with molecule−molecule, ion−molecule, and ion−ion pairs.[21,26−30]

Recently, we prepared and explored two alcoholic electrolyte systems, namely, $ZnCl_2$−EG[30] and $ZnCl_2$−EtOH[21] mixtures in a wide range of concentrations. For the $ZnCl_2$−EG mixtures,[30] the analysis of the excess infrared (IR) spectra assisted by quantum chemical calculations helped us to provide molecular-level evidence on the specific behavior of $ZnCl_2$−4EG mixture as the eutectic composition. We also found that through the dissolution of $ZnCl_2$ in EG, the EG multimer represented with tetramer is broken to EG dimer and EG trimer together with the formation of $ZnCl_2$−4EG complex. For the $ZnCl_2$−EtOH system,[21] the application of the same methods enabled us to provide a clear picture of the solvation process of $ZnCl_2$ in EtOH which paved the way to explain the microscopic reason behind the reduced vapor pressure of the mixtures compared with pure EtOH. Further analysis showed a transformation from EtOH trimer and EtOH tetramer to EtOH monomer, EtOH dimer, and $ZnCl_2$−3EtOH complex upon dissolution of $ZnCl_2$ in EtOH. In the current study, we decided to investigate $ZnCl_2$−MeOH mixtures. MeOH as the simplest alcohol is a highly structured liquid and capable of developing H-bonds to form, preferably, chains of clusters.[31−35]

The mixtures of MeOH with a variety of liquids[36−45] and salts[2,3,22,26,46−51] have been previously prepared to study either their physicochemical properties or, to a much lesser extent, microscopic nature. Regarding the microscopic behavior of MeOH electrolyte solutions, 1 and 2 M solutions of the $CaCl_2$−MeOH system were subjected to X-ray and neutron diffraction analysis together with molecular dynamics (MD) simulations.[48] It was found that the Ca−O distance is 2.43 Å; the coordination number of Ca^{2+} decreases with its concentration increase, which is due to the loss of solvating molecules. However, Cl^- ions keep a coordination number of six at both concentrations. In another study, excess Raman spectroscopy was employed to investigate the effects of $LiClO_4$, $NaClO_4$, $Mg(ClO_4)_2$, $LiNO_3$, NaCl, and LiCl salts on the microstructures of MeOH.[49] From the analysis of ν(O−H) region, it was found that the strength of the H-bonds in the solutions decreases as O−H···O−H > Cl^-···H−O > NO_3^-···H−O > ClO_4^-···H−O. Moreover, it was found that the ν(C−O) increases in the following order: anions···O−C < O−C_{bulk} < cations···O−C. The pyrimidine−MeOH mixtures are the other system whose H-bonding properties were explored by Raman spectroscopy and quantum calculations.[50] The results showed the presence of three spectral components in the ring-breathing region (1020−970 cm^{-1}), which were assigned to free pyrimidine, pyrimidine with low MeOH content, and pyrimidine with high MeOH content.

To the best of our knowledge, there is no report yet on the $ZnCl_2$−MeOH system, which is the system of focus in the present study to discuss it at the molecular level. Such study appears more urgent when knowing that the $ZnCl_2$−MeOH, $ZnBr_2$−MeOH, and LiBr/$ZnCl_2$−MeOH solutions have been suggested as potential heat transfer fluids for absorption refrigeration machines and heat pumps.[47,52] The reason is the improved thermal properties and reduced vapor pressure of $ZnCl_2$−MeOH and $ZnBr_2$−MeOH solutions compared with the aqueous solutions.[47] Moreover, the $ZnCl_2$−MeOH mixtures have been used as the titrant to titrate triblock copolymer elastomers (TBCPEs)−chloroform solutions during the experiment of synthesizing supramolecular TBCPEs with enhanced properties.[53] The $ZnCl_2$−MeOH mixtures in combination with dichloromethane, known as weak-associated electrolyte (WASE), have shown promising applications in Zn batteries with favorable properties such as high reversible Zn plating/stripping at low temperatures.[54] In one study to synthesize biodiesel, $ZnCl_2$ was added to canola oil-containing MeOH to catalyze the transesterification process.[55] In another study, two Zinc(II) complexes, namely, $[Zn(MPCA)_3][ZnCl_4]$ and $[Zn(MPCA)_3][ZnBr_4]$ (MPCA = O-methylpyridine-2-carboximidate), with several favorable applications were synthesized through the interaction of $ZnCl_2$ and $ZnBr_2$ with 2-pyridinecarbonitrile in methanol.[56] Moreover, the combination of MeOH and ChCl has been found to form DES with favorable applications.[22] This makes the exploration of other salt-containing MeOH solutions potential LoMMSs of value.

In this work, we aim to provide a description of the spectral, structural, and thermal properties of $ZnCl_2$−MeOH mixtures over a wide range of concentrations. To this purpose, attenuated total reflection Fourier transform infrared (ATR-FTIR), density functional theory (DFT), and differential scanning calorimetry (DSC) methods were employed. Because the initial IR spectra of the mixtures were highly overlapped, two resolution-enhancing methods, namely, excess absorption spectroscopy[57−59] and two-dimensional correlation spectroscopy (2D-COS)[60] were used to help in peak assignments.

MATERIALS AND METHODS

Materials and Sample Preparation. Methanol (MeOH, CH_3OH, >99.5%) and zinc chloride ($ZnCl_2$, >99.9%) were purchased from Beijing Chemical Plant (Beijing, China) and used without any further purification. For ATR-FTIR measurement, one series of $ZnCl_2$−MeOH mixtures with molar ratios from 1:14 to 1:3, corresponding to $ZnCl_2$ concentration from ∼6.7 to 25 mol %, were prepared by weighing. For the measurement of DSC thermograms, samples with molar ratios from 1:9 to 1:3 were prepared.

Spectroscopic Measurements. *ATR-FTIR Spectroscopy.* A Nicolet 5700 FTIR spectrometer equipped with a mercury−cadmium−telluride (MCT) detector and a Ge ATR with an incident angle of 60° and 7 reflections were employed to measure the FTIR spectra at room temperature. The spectra were recorded with a resolution of 2 cm^{-1} and 32 parallel scans. For the measurement of the refractive index of all of the mixtures, an Abbe refractometer was used at room temperature. For ATR corrections and calculation of light penetration depth, the formula suggested by Hansen was used.[61]

Excess IR Spectroscopy. The whole theory of excess IR spectroscopy which resembles the thermodynamic concept of excess functions can be traced in the literature.[57,62,63] Very concisely, an excess spectrum of a binary mixture at a given temperature and pressure is formulated in eq 1 and defined as the residue when the spectrum of the mixture is subtracted by the corresponding imaginary ideal mixture.

$$\varepsilon^E = \frac{A}{d(C_1 + C_2)} - (x_1\varepsilon_1^* + x_2\varepsilon_2^*) \quad (1)$$

where A is the absorbance of the mixture, C_1 and C_2, and x_1 and x_2 are, respectively, the molarities and mole fractions of the components, d is the light path length, and ε_1^* and ε_2^* are the molar absorptivity values of pure chemicals. Since in a binary mixture, $A = A_1 + A_2$, $x_1(C_1 + C_2) = C_1$, and $x_2(C_1 + C_2) = C_2$, eq 1 can be rearranged into the following form

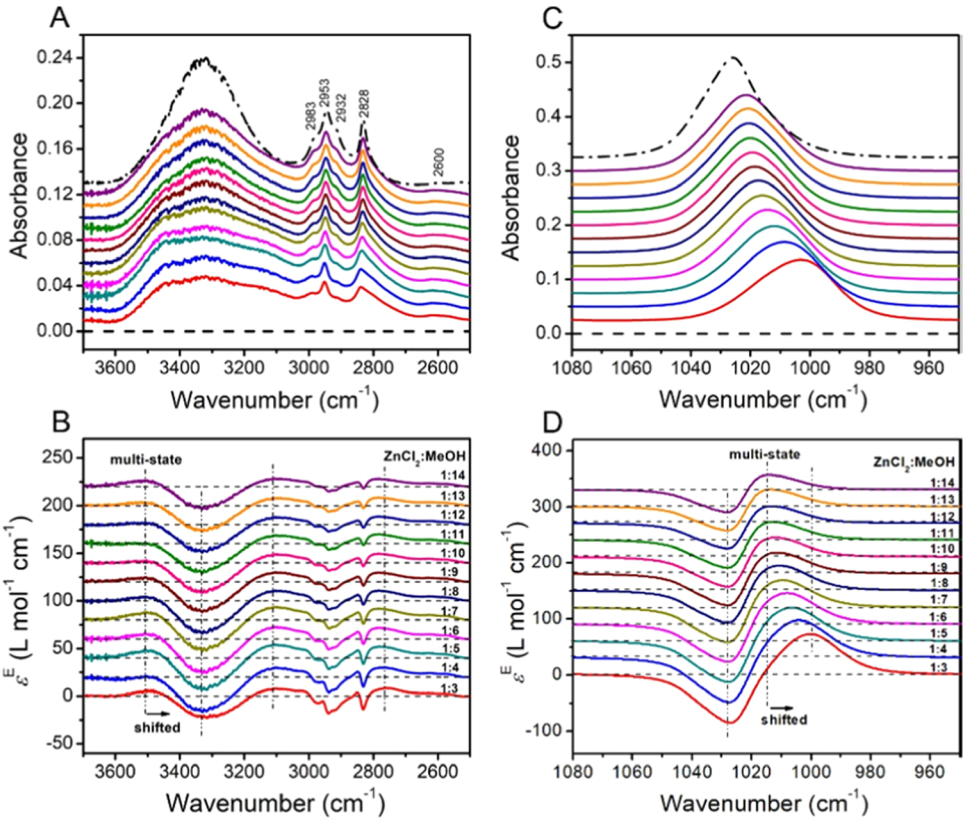

Figure 1. ATR-FTIR (A, C) and excess IR (B, D) spectra of $ZnCl_2$−MeOH mixtures in ν(O−H) and ν(C−H) (A, B) and ν(C−O) (C, D) regions. The dashed and dash-dotted spectra in parts (A, C) are for pure $ZnCl_2$ and MeOH, respectively. The molar ratios of the two components are labeled in (B, D). For clearer presentation, the baselines of the spectra at different concentrations have been shifted.

$$\varepsilon^{E} = x_1\left(\frac{A_1}{dC_1} - \varepsilon_1^*\right) + x_2\left(\frac{A_2}{dC_2} - \varepsilon_2^*\right)$$
$$= x_1(\varepsilon_1 - \varepsilon_1^*) + x_2(\varepsilon_2 - \varepsilon_2^*) \quad (2)$$

In the present study, the spectral regions of interest are contributed only by MeOH. Therefore, $x_2(\varepsilon_2 - \varepsilon_2^*) = 0$. Now, by defining $\varepsilon_d = (\varepsilon_1 - \varepsilon_1^*)$,[64] we obtain

$$\varepsilon_d = \frac{\varepsilon^{E}}{x_1} \quad (3)$$

Here, ε_d, called absorptivity deviation, measures the deviation of ε_1 in the binary mixture from its pure state and can be employed to quantitatively assess the variations of the amount of different H-bonded species.[21,30,64,65] The deconvolution of the excess spectra was carried out using PeakFit 4.0 software, with the Gaussian + Lorentzian area functions chosen for the best-fit procedure. Through the deconvolution process, the three fit parameters of the peaks, namely, position, intensity, and full width at half-maximum (fwhm) were set free to change.

Two-Dimensional Correlation Spectroscopy. The 2D Shige software (Shigeaki Morita, Kwansei-Gakuin University) based on the algorithm developed by Noda[60] was used to perform 2D-COS in ν(O−H), ν(C−H), and ν(C−O) spectral regions of MeOH. In order to have 2D-COS signals with variations only influenced by the intermolecular interactions, a method known as modified component-normalization[66] was used. In this method, the ν(O−H), ν(C−H), and ν(C−O) bands in the initial IR spectra were divided by the molarity of MeOH.

DSC Measurement. DSC Q200 from TA Instruments Inc. was employed to study the thermal behavior of the 1:9−1:3 molar ratio mixtures of the $ZnCl_2$−MeOH system (equivalent to 10−25 mol % of $ZnCl_2$). The samples of ∼4 mg were sealed in aluminum pans with an empty pan as the reference. A scan rate of 5 °C/min was selected for cooling the samples from 25 to −150 °C, with a subsequent heating back to 25 °C after an incubation time of at least 15 min. The TA Universal Analysis software was used for part of the analysis.

Theoretical Calculations. *Quantum Chemical Calculations.* For isolated $ZnCl_2$ and MeOH molecules and their complexes at different molecular ratios, several properties, namely, vibrational frequencies, stabilization energies, and electrostatic potential maps were calculated from the obtained most stable geometries optimized using Gaussian 09.[67] Two levels of theory B3LYP-D3/6-311++G(d,p) and M06-2X/6-311++G(d,p) which are frequently used to study intermolecular interactions in alcoholic systems[21,28,30,43,68−71] were employed for the calculations both in the gas phase and under solvent effect. For the solvent effect calculations, the conductor-like polarizable continuum model (cpcm) was employed.[72] Moreover, to obtain accurate interaction energies, basis set superposition error (BSSE) corrections based on the counterpoise (CP) method were carried out.[73] In addition, for the components of interest, the Hirshfeld charges[74] and topological properties based on the atoms in molecules (AIM) theory[75] were calculated using the Multiwfn program, version 3.8.[76]

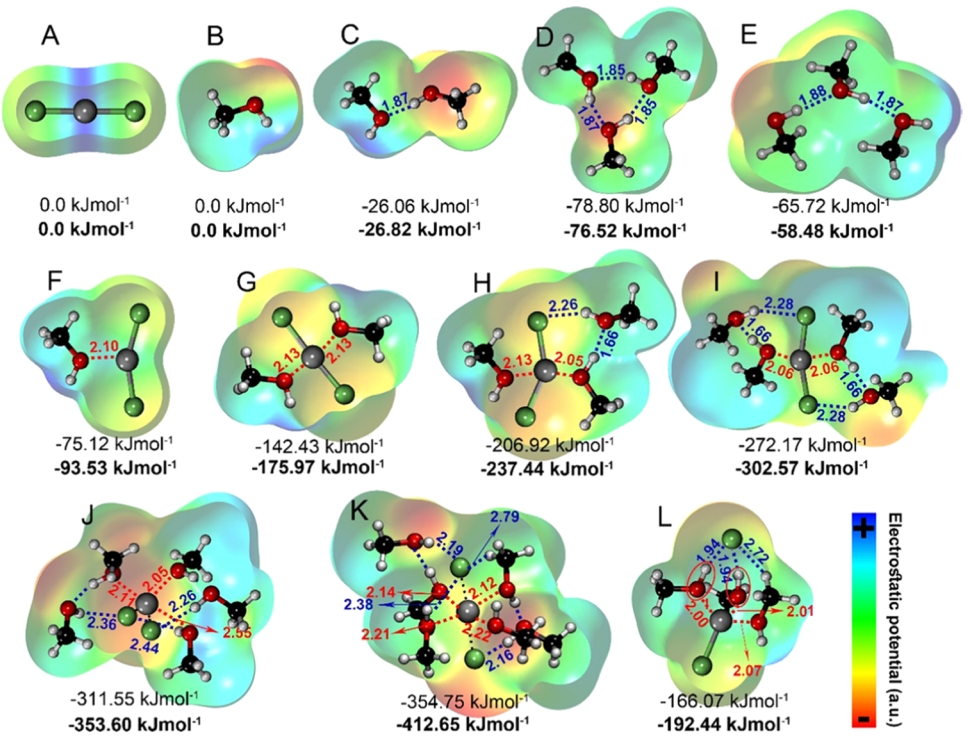

Figure 2. Optimized geometries and relative interaction energies of $ZnCl_2$ (A), monomer to trimer of MeOH (B–E), $ZnCl_2$–*n*MeOH complexes with *n* = 1–6 (F–K) and a 1:3 molecular ratio complex containing largely red-shifted hydroxyls (L). The optimization was at the B3LYP-D3/6-311++G(d,p) level of theory in the gas phase. The interaction energies in bold were calculated at the M06-2*X*/6-311++G(d,p) level of theory in the gas phase. The blue and red broken lines indicate, respectively, the lengths of H-bonds and Zn ← O coordination bonds in the unit of angstrom (Å). The black broken lines between the Zn and Cl atoms in complexes (J) and (K) represent the broken bonds. Electrostatic potentials are represented with colors on the molecular vdW isosurfaces.

RESULTS AND DISCUSSION

Experimental Analysis of the Interactions between $ZnCl_2$ and MeOH.

ATR-FTIR Analysis of ν(O–H), ν(C–H), and ν(C–O). Figure 1A,C shows the IR spectra of $ZnCl_2$–MeOH mixtures in ν(O–H) and ν(C–H) regions (Figure 1A) and ν(C–O) region (Figure 1C) with the $ZnCl_2$ mol % increasing from ∼6.7 (1:14 molar ratio) to 25 (1:3 molar ratio) along with the IR spectra of pure $ZnCl_2$ (dash spectrum) and MeOH (dash-dotted spectrum). MeOH has distinctive bands, namely, a broad one in ν(O–H) region extending from ∼3650 to 3050 cm^{-1} and several smaller bands in ν(C–H) region extending from ∼3050 to 2800 cm^{-1} (Figure 1A) together with a band in ν(C–O) region at around 1026 cm^{-1} (Figure 1C). The band in ν(O–H) region is centered at ∼3330 cm^{-1} and is closely associated with the extensive H-bonds in the liquid. Regarding ν(C–H) region, the most prominent bands are the ones at 2953 and 2828 cm^{-1}, which are attributed to ν_{as}(C–H) and ν_s(C–H), respectively.[31,77,78] There are two shoulders at 2983 and 2932 cm^{-1} which are assigned to another low-intensity vibration mode of ν_{as}(C–H)[33] and overtones of $2\delta(CH_3)$,[33] respectively. Finally, the blunt band at the lowest region of the spectrum at ∼2600 cm^{-1} is attributed to the combination of $\delta_{as}(CH_3)$ and rocking-(CH_3) bands.[31] By addition of $ZnCl_2$, the shapes, wavenumbers, and intensities of the MeOH bands change, indicating that the local structures in MeOH are modulated by the solvation interactions. Here, the formation of new species (associates, complexes, or clusters) is revealed by the wavenumber shifts or appearance of shoulders. The two prominent bands in ν(C–H) region, namely, ν_{as}(C–H) and ν_s(C–H), are blue-shifted by the addition of $ZnCl_2$. Here, the blue shift represents the strengthening of the respective H-bonds as C–Hs of MeOH are improper H-bond-formation groups.[79]

Moreover, in $ZnCl_2$–MeOH mixtures, a low-intensity broadband at ∼2780 cm^{-1} appears. This band can be assigned to the largely red-shifted hydroxyls (LRS–OHs) of MeOH molecules interacting with the dissociated components of $ZnCl_2$ in the specific geometry of $Cl–Zn^+\cdots O–H\cdots Cl^-$ (see Density Functional Theory section). Similar bands have been previously reported by the authors for $ZnCl_2$–EG[30] and $ZnCl_2$–EtOH[21] mixtures or by others for the aqueous solutions of ChCl–xylitol and ChCl–glucose DESs.[80] Moreover, the IR predissociation (IR-PD) experiment combined with ab initio MD simulations have shown a large red shift of ν(O–H) in MeOH, which has a direct H-bond to Cl^- in $Cl^-\cdots(MeOH)_2$ complex to vibrate at around 2844 cm^{-1} (MD) or 2819 cm^{-1} (IR-PD).[81] In the ν(C–O) region (Figure 1C), the bands are red-shifted under the effect of $ZnCl_2$ mixing. This suggests the weakening of the C–O bond, very possibly due to the electron depletion of oxygen when interacting with the surrounding electron acceptor species.

Despite all of the useful information gained from the spectral changes of the initial IR spectra, it is still impossible to draw a clear picture of the underlying transformations between the most probable species in solutions. In this regard, excess absorption spectroscopy has been proven to be the method of choice for its provision with higher resolution spectra compared with the initial spectra.[28,65,70,82,83] An excess spectrum is normally composed of at least one positive and one negative peak to represent, respectively, the appearance/

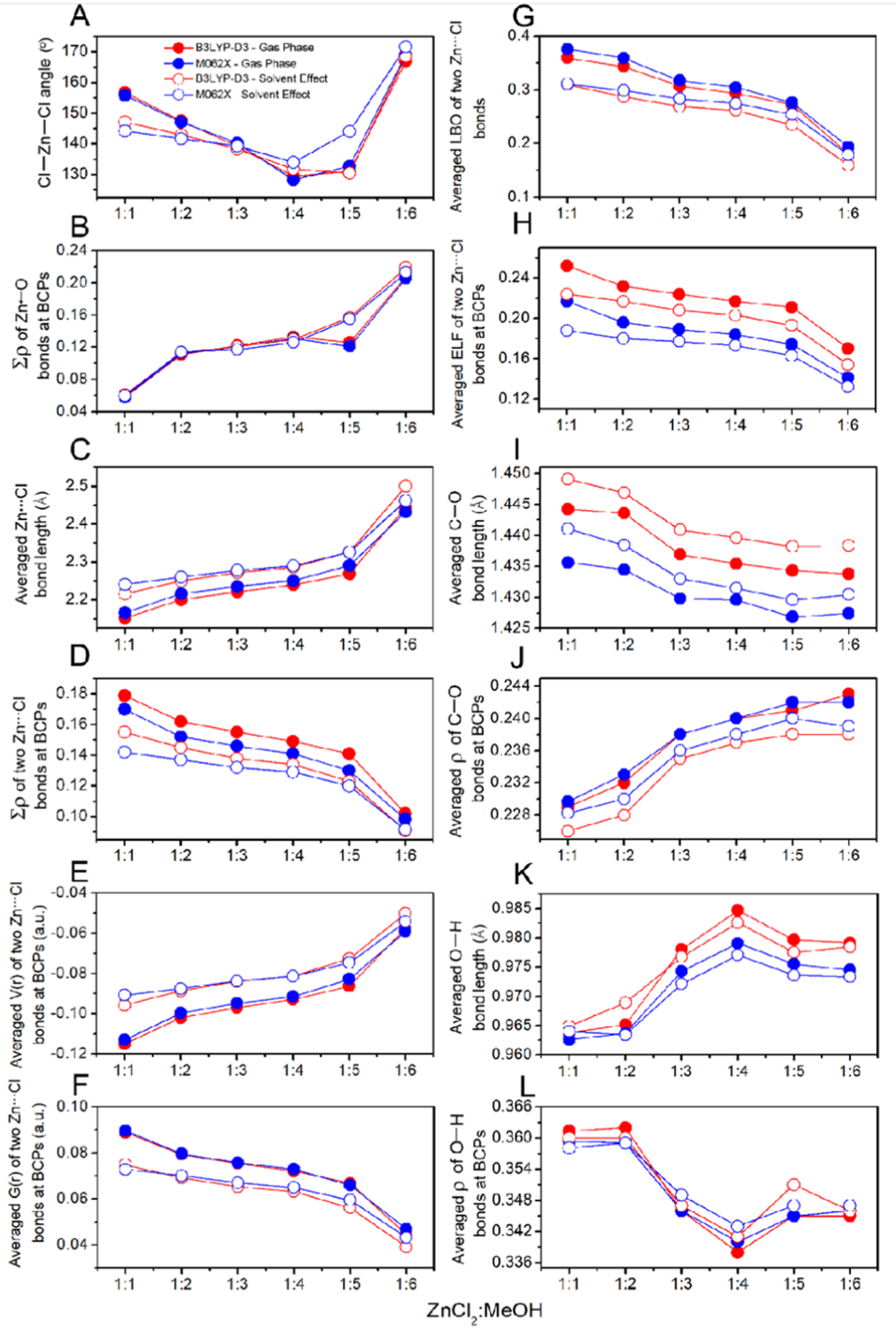

Figure 3. Cl−Zn−Cl angles (A), $\sum\rho_{BCPs}$ of Zn ← O coordination bonds (B), averaged Zn···Cl bond lengths (C), $\sum\rho_{BCPs}$ of Zn···Cl bonds (D), averaged V_{BCPs} of Zn···Cl bonds (E), averaged G_{BCPs} of Zn···Cl bonds (F), averaged LBO of Zn···Cl bonds (G), averaged ELF_{BCPs} of Zn···Cl bonds (H), averaged C−O bond lengths (I), averaged ρ_{BCPs} of C−O bonds (J), averaged O−H bond lengths (K), and averaged ρ_{BCPs} of O−H bonds (L) vs 1:1−1:6 molecular ratios of $ZnCl_2$−MeOH complexes. The results are associated with structures (F−K) in Figure 2 optimized at B3LYP-D3 and M06-2X levels in the gas phase and under the solvent effect. The topological results (panels B, D−H, J, and L) were obtained from AIM calculations.

increasing amount and disappearance/decreasing amount of the relevant species in the mixtures relative to the linear values upon mixing. Figure 1B shows the excess spectra of the mixtures in ν(O−H) and ν(C−H) regions with multiple positive and negative peaks. Among the excess bands in ν(O−H) region, the one at the highest wavenumbers shifts rightward upon the addition of $ZnCl_2$ to signal a multistate transformation.[84] This peak together with the other positive peak just on the right of the large negative peak in the ν(O−H) region is indicative of the newly formed MeOH-containing species with weaker and stronger H-bonds than those in pure MeOH, respectively. In both ν_s(C−H) and ν_{as}(C−H) regions, positive bands are followed by negative bands to indicate newly formed species with blue-shifted C−Hs. The excess spectra in

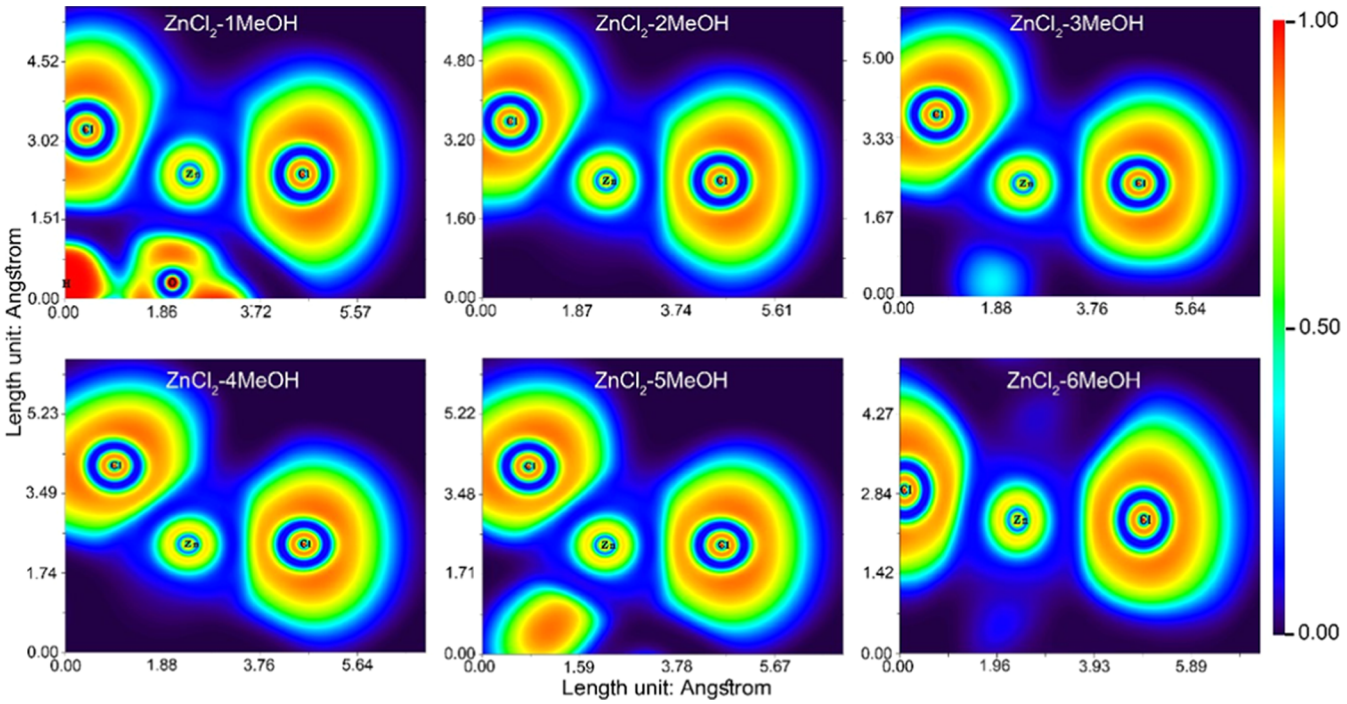

Figure 4. ELF maps along the Cl−Zn−Cl plane of 1:1−1:6 molecular ratios of $ZnCl_2$−MeOH complexes. The optimization was at B3LYP-D3/6-311++G(d,p) level of theory in the gas phase.

the ν(C−O) region (Figure 1D) reveal a negative peak followed by a multistate positive peak, suggesting the formation of at least two MeOH-containing species with weakened C−O bonds.

Theoretical Investigation on the Interactions between $ZnCl_2$ and MeOH. *Density Functional Theory.* Quantum chemical calculations were employed to obtain a molecular-level understanding of the primary solvation shell of $ZnCl_2$ in $ZnCl_2$−*n*MeOH (n = 1−6) complexes and to predict the most probable structures and their associated prominent interactions. Moreover, the monomer to trimer of MeOH were explored. Following our previously undertaken procedure,[21,30] the structures were first optimized at the B3LYP/6-311++G(d,p) level of theory after which the most stable ones were reoptimized at B3LYP-D3/6-311++G(d,p) and M06-2X/6-311++G(d,p) levels of theory in the gas phase and under solvent effect. The most stable structures from the two levels of theory, either in the gas phase or under the solvent effect, have close geometries but with discrepancies in interaction energies and vibrational frequencies. The main motivation to use more than one functional is to solidify our conclusions. By doing so, we make sure that the conclusions drawn are not overly dependent on the choice of functional. Figure 2 shows some selected structures of the favorable species optimized at the B3LYP-D3/6-311++G(d,p) level of theory in the gas phase. To judge the formation of H-bonds, the sums of the van der Waals radii ($\sum r_{vdW}$) of the interacting atoms, namely, H and O (2.5 Å) and H and Cl (3.0 Å), were considered as criterion values.[85] Besides, the $\sum r_{vdW}$ of O and Zn (2.91 Å)[86] and $\sum r_{covalent}$ of Cl and Zn (2.24 Å)[87] were used as critical values for the formation of coordination (spodium) and covalent bonds, respectively.

Shown in Figure 2A,B are the monomers of $ZnCl_2$ and MeOH, respectively. The MeOH dimer (complex C) and two geometries of the MeOH trimer, namely, the cyclic (complex D) and chain (complex E) structures, are also shown in Figure 2. It is worth noting that despite the higher stability of the cyclic structure (complex D) than the chain one (complex E) when comparing their stabilization energies, the reported neutron scattering and X-ray scattering results[88] on pure MeOH suggest the predominance of chain trimer and tetramer of MeOH in pure state. This might be due to the high constraint of the small ring in the cyclic structure.

The most stable structures of $ZnCl_2$−MeOH complexes found in this work at different molecular ratios are given in Figure 2F−K. In these complexes, the two major intermolecular interactions are H-bonds (O−H···O, O−H···Cl, C−H···Cl) and coordination bonds (Zn ← O) which are shown by blue and red dashed lines, respectively. It is widely discussed that the H-bond formation between the H-bond donor (MeOH in the present case) and the H-bond acceptor ($ZnCl_2$ in the present case) and the subsequent charge transfer result in the DES formation.[21,28,30,70,89−92] The coordination number of Zn increases from 1 in a 1:1 molecular ratio complex (complex F) to 2 in 1:2−1:4 molecular ratio complexes (complexes G−I), then to 3 in a 1:5 molecular ratio complex (complex J), and 4 in a 1:6 molecular ratio complex (complex K). This is accompanied by the continuous reduction in the Cl−Zn−Cl angle from 180° in isolated $ZnCl_2$ (structure A) to less than 145° in 1:4 (complex I) or 1:5 (complex J) molecular ratio complexes, as is shown in Figure 3A. Based on Figure 3B, the electron density at bond critical points (ρ_{BCP}) of Zn ← O coordination bonds also increases (with the exception of deviation for the gas phase calculations for $ZnCl_2$−5MeOH complex) from 1:1 to 1:6 molecular ratio complexes (complexes F−K). Such deformation of $ZnCl_2$ in $ZnCl_2$−MeOH complexes is similar to those reported for other systems, namely, $ZnCl_2$−EtOH,[21] $ZnCl_2$−EG,[30] and $ZnCl_2$−carbene/carbodiphosphorane.[93] According to Figure 3C, the averaged Zn−Cl bond length in each complex from 1:1 to 1:6

molecular ratios (complexes F−K) increases monotonically, which is accompanied by the reduction of ρ_{BCP} of Zn−Cl bonds (Figure 3D). As can be seen in $ZnCl_2$−5MeOH (Figure 2J) and $ZnCl_2$−6MeOH (Figure 2K) complexes, the Zn−Cl bonds are broken (shown by black broken lines), indicating the Zn···Cl distance is beyond the $\sum r_{covalent}$ of Cl and Zn (2.24 Å).[87] This happens together with the abrupt increase of the Cl−Zn−Cl angle (Figure 3A) and the drop of ρ_{BCP} of Zn···Cl bonds (Figure 3D) in 1:5 and 1:6 molecular ratio complexes. These all suggest the Zn−Cl bond dissociation. Furthermore, as shown in the Supporting Information (Figure S1), the theoretical ν(Zn−Cl) decreases from 1:1 to 1:4 molecular ratio complexes (the Zn−Cl bonds are broken in 1:5 and 1:6 molecular ratio complexes), which is supportive of the Zn−Cl bond lengthening (Figure 3C). The lengthening of the Zn−Cl bonds and the consequent geometrical distortion of $ZnCl_2$ interacting with MeOH is similar to those reported for interactions between $BeCl_2$ and $MgCl_2$ with Lewis bases such as NH_3 to form Be ← N or Mg ← N coordination bonds.[94−96] The lengthening of the Zn−Cl bonds (Figure 3C) and decrease of the associated electron densities (Figure 3D) from 1:1 to 1:6 molecular ratio complexes are accompanied by the increase of the potential energy density at BCP (V_{BCP}) (Figure 3E) and decrease of the kinetic energy density at BCP (G_{BCP}) (Figure 3F) of Zn−Cl bond electrons. From 1:1 to 1:6 molecular ratio complexes, the increase of V_{BCP} values (Figure 3E) clearly shows the destabilization/weakening of the Zn−Cl bond. The decrease of G_{BCP} values (Figure 3F) suggests less mobility of electrons as a result of the gradual decrease of covalency and increase of ionic character of the Zn−Cl bond.

Moreover, depending on the $|V_{BCP}|/G_{BCP}$ ratio, the bond can be more electrostatic ($|V_{BCP}|/G_{BCP} < 1$), partially covalent ($1 < |V_{BCP}|/G_{BCP} < 2$), or highly covalent ($|V_{BCP}|/G_{BCP} > 2$) in nature.[97] In the present study, the $|V_{BCP}|/G_{BCP}$ ratio for each Zn−Cl bond in all of the 1:1−1:6 molecular ratio complexes was found to be around 1.29 au at the B3LYP-D3 functional and 1.25 au for the M06-2X functional, regardless of the phase of the calculations. This suggests the partially covalent nature of the Zn−Cl bond. The Laplacian bond order (LBO) is a measure of covalency.[98] As shown in Figure 3G, from 1:1 to 1:6 molecular ratio complexes, the averaged LBO values of Zn:Cl bonds decrease to show a decrease of the Zn:Cl bond covalency. This observation is supported by the decrease of the electron localization function (ELF) values at BCPs (ELF_{BCPs}) of the Zn−Cl bonds (Figure 3H) from 1:1 to 1:6 molecular ratio complexes. The higher values of ELF_{BCPs} show that electrons are more localized[99] and bonds are more covalent. The respective ELF maps in Figure 4 represent the spread of electron localization through the Cl−Zn−Cl plane. The scale bar spans from highly localized (red color) to totally delocalized (dark blue color) electrons. It is noticed that in all of the complexes, the color through Zn−Cl bonds is light blue, suggesting that the bond electrons are not highly localized. In addition, the magnitude of the light blue color decreases from 1:1 to 1:6 molecular ratio complexes and a dark blue color appears instead. This implies the increase of electron delocalization as a consequence of covalency decrease. Additionally, the ELF maps show the changes in Cl−Zn−Cl angles, consistent with Figure 3A. Regarding the C−O bond length in MeOH, the experimental values obtained by neutron scattering and X-ray diffraction are 1.435[88] and 1.437 Å.[100] Among the different computational methods used in the present work, the best approximation was from the B3LYP-D3/6-311++G(d,p) level of theory under the solvent effect with an average C−O bond length of 1.430 Å for both the chain and cyclic MeOH trimers. Figure 3I shows that upon addition of MeOH molecules to $ZnCl_2$ from 1:1 to 1:6 molecular ratio complexes (complexes F−K), the C−O bond is shortened constantly (the exception is the results from the M06-2X level which shows subtle C−O lengthening for the $ZnCl_2$−6MeOH complex). This finding together with that on increase of ρ_{BCP} of C−O bonds (Figure 3J) from 1:1 to 1:6 molecular ratio complexes (complexes F−K) is consistent with our experimental results (Figure 1C) showing blue shifts of ν(C−O) when diluting the mixture with MeOH. The changes in O−H bond lengths and their respective ρ_{BCP} are shown in Figure 3K,L, respectively. As can be seen in Figure 3K, from 1:1 to 1:4 molecular ratio complexes (complexes F−I), the bond length increases together with the decrease of the ρ_{BCP} values (Figure 3L). However, for 1:5 and 1:6 molecular ratio mixtures (complexes J and K), the trend reverses in Figure 3K,L. The initial red shift of the hydroxyls and their consequent blue shift imply the strengthening and weakening of the H-bonds, respectively.

Complex L in Figure 2 shows a $ZnCl_2$−3MeOH complex where two of the hydroxyls are located between Cl−Zn^+ and Cl^- species to form Zn ← O coordination bonds and O−H···Cl H-bonds simultaneously. This makes the involved hydroxyls become largely red-shifted (LRS) (see section Assignments of the Experimental Excess Peaks ν(O−H) Region). We have previously reported similar phenomena for some hydroxyls in $ZnCl_2$−EG[30] and $ZnCl_2$−EtOH[21] systems. The excess band appearing at 2780 cm^{-1} (Figure 1B) is suggested to be ascribed to such LRS−OHs.

Charge Transfer Analysis. Shown in Figure 5 are the Hirshfeld charges[74] on Zn, Cl, $ZnCl_2$, and MeOH species in monomeric states (Figure 2A,B) and in $ZnCl_2$−MeOH complexes (Figure 2F−K) calculated at the B3LYP-D3/6-311++G(d,p) level of theory in the gas phase and under solvent effect. Similar calculations are performed at the M06-2X/6-311++G(d,p) level of theory and given in the Supporting Information (Figure S2). It is readily seen that the Zn and Cl atoms in the $ZnCl_2$ monomer carry positive and negative charges, respectively. It suggests the Zn−Cl bonds are polar. As the MeOH molecules are added stepwise, the initially neutral $ZnCl_2$ and MeOH molecules are charged negatively and

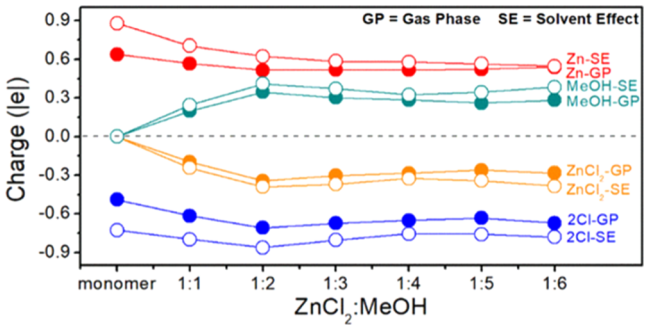

Figure 5. Hirshfeld charges on selected atoms and molecules vs $ZnCl_2$, MeOH, and 1:1−1:6 molecular ratios of $ZnCl_2$−MeOH complexes. The results are associated with structures (A−K) in Figure 2 optimized at the B3LYP-D3 level in the gas phase and under solvent effect (results at the M06-2X level are given in Figure S2). The atomic charges of Zn-SE/GP are increased by 0.15 for better representation.

positively, respectively. From 1:1 to 1:6 molecular ratio complexes (complexes F−K in Figure 2), the Zn atoms are increasingly receiving negative charge. This is in good agreement with the gradual increase of $\sum\rho_{BCP}$ of Zn ← O coordination bonds under the solvent effect (Figure 3B) and the increase of Zn coordination numbers from 1 in the 1:1 molecular ratio complex (complex F) to 4 in the 1:6 molecular ratio complex (complex K). In 1:1 and 1:2 molecular ratios of $ZnCl_2$−MeOH complexes (complexes F and G) where only Zn ← O coordination bond(s) exist, Cl atoms receive progressively negative charge from Zn atoms. However, in 1:3−1:6 molecular ratio complexes (complexes H−K) with H-bonds, Cl atoms become less negative. This clearly indicates the partial return of the negative charge acquired by Zn atoms through Zn ← O coordination bonds back to MeOH molecules via the formation of O−H···Cl H-bonds. However, although the H-bonds and other molecular orbital interactions contribute to charge transfer between species, the major channel for charge transfer is the formation of Zn ← O coordination bonds. This is understood by the final negative charge of the $ZnCl_2$ molecules. A similar phenomenon has been previously reported by the authors for $ZnCl_2$−EG[30] and $ZnCl_2$−EtOH[21] mixtures. Moreover, non-negligible amounts of charge transferred from some Lewis bases to Lewis acid centers, namely, $ZnCl_2$, $BeCl_2$, and $MgCl_2$, have been previously reported.[93−96]

Assignments of the Experimental Excess Peaks at ν(O−H) Region. For a deeper understanding of the structural transformations in solutions, we begin further analysis of the obtained excess spectra with the help of the aforementioned quantum calculations. The analysis starts with the deconvolution of the excess spectra in ν(O−H) and ν(C−H) regions (Figure 1B), guided by their positive and negative peaks. Since the ν(C−H) region is very overlapped, the peak assignment of the region is not considered. In this regard, the excess bands with fixed positions were deconvoluted to one peak, and the one with a drifting position located at the highest wavenumbers was deconvoluted to two peaks to obtain the best fitted spectra. Figure 6A represents the deconvoluted excess spectrum of the $ZnCl_2$−3MeOH mixture. For other mixtures, the deconvolution results are given in the Supporting Information (Figure S3). Totally, five peaks were derived through deconvolution, four of them can be found within the O−H region, approximately ranging from 3650 to 3050 cm^{-1}, while the remaining deconvoluted peak is situated below the C−H region. The excess peak assignments are assisted by the quantum calculations. Figure 6B shows the linear correlations between the experimental wavenumbers of the deconvoluted excess peaks and the theoretical wavenumbers of some of the selected structures. It is seen that the correlation coefficients are good enough to validate the assignments. This method of peak assignment has been previously proposed in our group[101] and then was frequently adopted for excess peak assignment.[21,28,30,59,65,70] As is clearly shown in Figure 6B, the excess peak assignments are as follows: the negative excess peak at 3340 cm^{-1} is assigned to pure MeOH, which is represented by the MeOH chain trimer (complex E in Figure 2). After $ZnCl_2$ is mixed with MeOH, the larger oligomers of MeOH are broken to produce smaller aggregates along with $ZnCl_2$−MeOH complexes. Accordingly, the two positive excess peaks at 3530 and 3435 cm^{-1} are assigned to the appearing MeOH monomer (structure B) and MeOH dimer (complex C). A previous study has shown the presence of ∼2.5% monomers

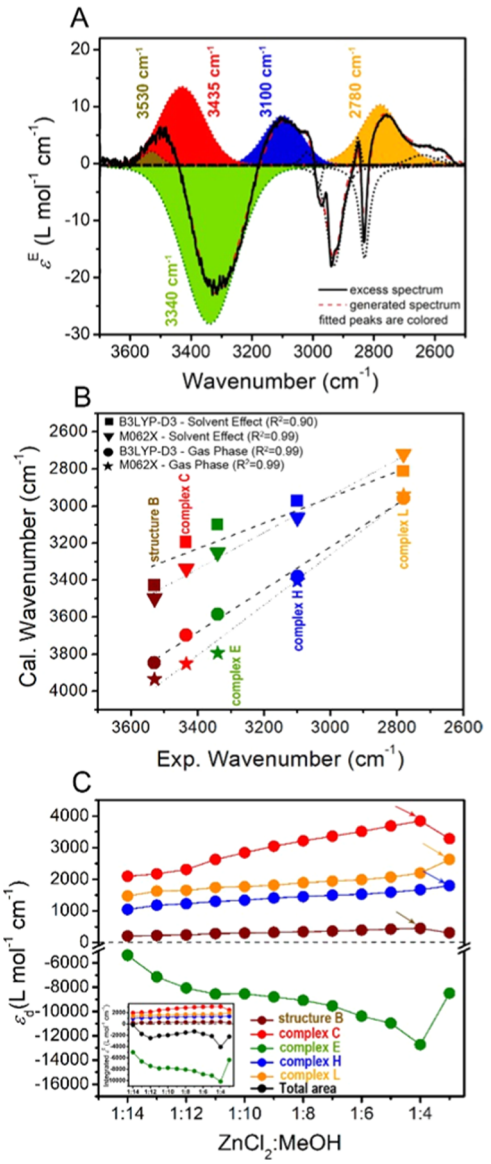

Figure 6. Deconvolution results of the excess spectrum of $ZnCl_2$−3MeOH mixture (A), the relationship between the experimental wavenumbers from the deconvoluted excess peaks and the selected theoretical results at B3LYP-D3 and M06-2X levels (B), and concentration-dependent molar absorptivity deviation of the hydroxyl-containing deconvoluted excess peaks (C). The inset in (C) shows the concentration dependence of the integrated areas of the hydroxyl-containing deconvoluted excess peaks. The wavenumbers calculated at B3LYP-D3 and M06-2X levels with the solvent effect method were subtracted by 400 cm^{-1} to distinguish them from those of the gas phase (B).

and no indication of MeOH dimer in pure MeOH.[102] The two remaining excess peaks at 3100 and 2780 cm^{-1} are attributed to the $ZnCl_2$−3MeOH complex without and with LRS−OHs, i.e., complexes H and L in Figure 2, respectively. Although both B3LYP-D3 and M06-2X functionals yield similar trends in terms of reproducing the vibrational frequencies (Figure 6B), the higher R^2 value of the M06-2X functional for the calculations under solvent effect may imply a better performance for the present system. It has been already reported that the vapor pressure of $ZnCl_2$−MeOH mixtures with different molalities is significantly reduced compared with pure MeOH.[46,47] This phenomenon highlights the importance of

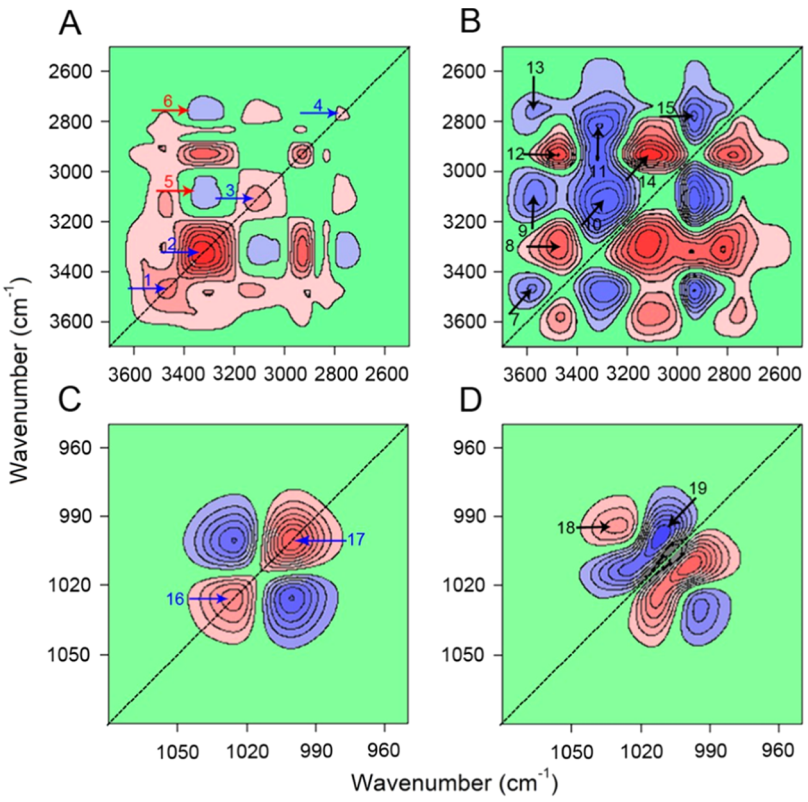

Figure 7. Synchronous (A, C) and asynchronous (B, D) 2D-COS contour maps of ν(O−H) and ν(C−H) (A, B) and ν(C−O) (C, D) in the process of increasing concentration of $ZnCl_2$. Red and blue maps represent positive and negative correlation intensities, respectively.

mixing MeOH with appropriate salts to, on one side, reduce the hazardous effect of volatile MeOH and, on the other side, increase the applicability of the solvent.[47,103−108] The present data on the formation of coordination bonds and H-bonds between $ZnCl_2$ and MeOH components such as complexes H and L in Figure 2 are the most likely reason behind the reduction of the vapor pressure of the mixtures compared with MeOH. It is worth mentioning that to construct the linear correlations (Figure 6B), the theoretical wavenumbers of the hydroxyls of relevant structures, except structures B and L, are intensity-weighed averages, following the literature method.[109]

The quantitative variations of the species identified in the mixtures are assessed using ε_d values, as shown in Figure 6C. In the figure, the positive points imply the formation or increasing amounts of the associated species, while the negative points suggest the dissociation or decreasing amounts of species. It is readily seen that from 1:14 to 1:4 molar ratios of $ZnCl_2$−MeOH mixtures, $ZnCl_2$ addition dissociates the MeOH trimer (complex E in Figure 2) increasingly. This is accompanied by increasing the quantities of all other identified species, but in different amounts. Namely, MeOH monomer (complex B) and MeOH dimer (structure C) are the species with the lowest and highest quantities in the mixtures, respectively. They reach their maxima at the $ZnCl_2$−4MeOH mixture (red and brown arrows) where the MeOH trimer (complex E) is at minimum. The minimum value of the MeOH trimer (complex E) in the $ZnCl_2$−4MeOH mixture means the highest impact of $ZnCl_2$ on the H-bonding network of pure MeOH among the studied mixtures. Moreover, the maximum values of the MeOH monomer (structure B) and MeOH dimer (complex C) imply that the H-bonds in the $ZnCl_2$−4MeOH mixture are weakened to the highest extent. From $ZnCl_2$−4MeOH to $ZnCl_2$−3MeOH mixtures, the addition of $ZnCl_2$ appears less destructive to the pure bulk, but with quantities of $ZnCl_2$−3MeOH complexes (complexes H and L) to be the highest (orange and blue arrows). The inset of Figure 6C shows the concentration-dependent integrated areas of the deconvoluted excess peaks. It can be seen that the appearance of the curves is similar to that of the normal excess thermodynamic functions. However, since the nature of the two interacting components is highly different, the curves are asymmetric.

Two-Dimensional Correlation Spectroscopy. In order to draw more information from the IR spectra, the 2D-COS method was performed on the concentration-normalized initial IR spectra. Figure 7 shows the synchronous (A and C) and asynchronous (B and D) contour maps in ν(O−H) and ν(C−H) (A and B) and ν(C−O) (C and D) regions over the entire concentrations. In the synchronous map in ν(O−H) region (Figure 7A), four autopeaks marked by blue arrows and numbered from 1 to 4 match the four deconvoluted excess peaks in ν(O−H) region (Figure 6A), namely, MeOH dimer (complex C in Figure 2), MeOH trimer (complex E), $ZnCl_2$−3MeOH complex (complex H), and the LRS−OHs in $ZnCl_2$−3MeOH complex (complex L), respectively. The autopeak related to MeOH monomer (compound B) is buried under autopeak 1. It is noticed that in the same synchronous map, two cross peaks at (3340, 3100) cm^{-1} (arrow 5) and (3340, 2780) cm^{-1} (arrow 6) appear. The peaks are negative as the changing direction of ν(O−H) intensities are opposite. Here, the peak at 3340 cm^{-1} is assigned to the disappearing MeOH trimer (complex E) while the ones at 3100 and 2780 cm^{-1} are assigned to appearing $ZnCl_2$−3MeOH complexes (complexes H and L). The asynchronous map in ν(O−H) region (Figure 7B) with higher resolution than the synchronous one reveals

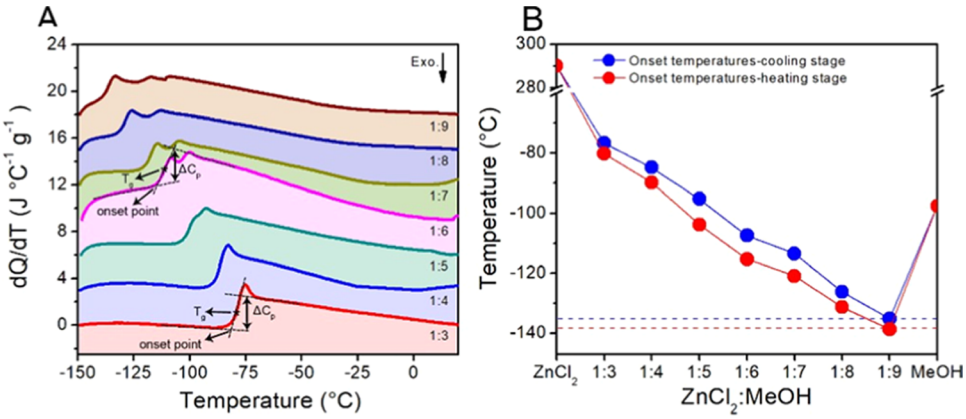

Figure 8. DSC thermograms between −150 and 20 °C for 1:3−1:9 molar ratios of $ZnCl_2$−MeOH mixtures (A) and the respective phase diagram of the mixtures based on the onset temperatures together with the melting points of pure components (B). Panel (A) shows the heating curves. The cooling curves are given in the Supporting Information (Figure S4). Each curve in (A) is normalized by the sample mass.

nine cross peaks at ∼(3560, 3450), (3450, 3326), (3560, 3100), (3326, 3100), (3326, 2780), (3450, 2934), (3560, 2780), (3100, 2934), and (2934, 2780) cm^{-1}, numbered from 7 to 15. Out of the six wavenumbers, five wavenumbers at 3560, 3450, 3326, 3100, and 2780 cm^{-1} have high correlation with those obtained from deconvolution of the excess spectrum (Figure 6A) with $R_{(excess\text{-}2D\text{-}COS)}{}^2 > 0.99$. The synchronous map in ν(C−O) region (Figure 7C) represents two autopeaks at (1026, 1026) cm^{-1} (number 16) and (1003, 1003) cm^{-1} (number 17), referring to the negative and positive excess bands observed in Figure 1D, respectively. The associated asynchronous map (Figure 7D) provides cross peaks at (1030, 996) cm^{-1} (number 18) and (1014, 996) cm^{-1} (number 19). The three wavenumbers at 1030, 1014, and 996 cm^{-1} correspond to three wavenumbers in ν(C−O) region of the excess spectra (vertical broken lines in Figure 1D) at 1028, 1015, and 999 cm^{-1} with $R_{(excess\text{-}2D\text{-}COS)}{}^2 > 0.99$.

Differential Scanning Calorimetry. DSC thermograms provide fingerprints of the materials' thermodynamic changes. Figure 8A shows the DSC data as heat capacity (C_p) normalized by the sample mass in the heating stage for 1:3−1:9 molar ratios of $ZnCl_2$−MeOH mixtures. Clear endothermic baseline shifts due to glass transitions (T_g) are found at ∼−78, −86, −100, −112, −118, −129, and −137 °C in the thermograms of 1:3 to 1:9 molar ratio mixtures. Here, the T_g at each thermogram represents a transition from a glassy crystalline phase to a liquid-like amorphous phase.[110] Although the melting points are absent, the V-shaped phase diagram allows us to classify the mixtures as LoMMSs, following our recent recommendation.[18] The thermograms of the same mixtures in the cooling stage are given in the Supporting Information (Figure S4). The onset temperatures of the observed T_g peaks in heating and cooling stages together with the melting points of the pure components are used to construct the phase diagram of the system as is shown in Figure 8B. The way the T_g and onset points were selected in this study are shown for 1:3 and 1:6 molar ratio mixtures in Figure 8A. The decrease of the onset temperature values upon MeOH addition (Figure 8B), which is probably due to the systematic change of the dominant intermolecular interactions and microstructures, has been previously reported for inorganic salt-containing amine or alcohol mixtures.[11] In the present DSC experiment, as the mixtures are diluted, a small second thermal peak or even third thermal peak (in the $ZnCl_2$−9MeOH mixture) appears. The reason for peak splitting is probably the increase of the heterogeneity of the mixtures with different local stoichiometries upon temperature decrease. A similar phenomenon has been previously reported for the imidazolium-urea LTTMs[111] and different DESs.[112] Moreover, a comparison between the low-frequency region of Raman spectra of the $ZnCl_2$−40MeOH mixture at 25 °C and in the glassy state ($T \approx -140$ °C) showed that the $ZnCl_2$-solvated species are the dominant complexes in the mixture at room temperature. While, in the glassy state, $ZnCl_3{}^{-1}$, $ZnCl_4{}^{-2}$, and $[Zn(MeOH)6]^{+2}$ species are the major structures.[113] This can be regarded as another proof of the increased heterogeneity and the consequent glass transition peak splitting of $ZnCl_2$−MeOH mixtures at low temperatures. In other words, in mixtures with lower contents of $ZnCl_2$, some microstructures of MeOH are preserved. This makes the mixtures more heterogeneous with their (split) T_g values approaching that of pure MeOH ($T_{g(MeOH)} \approx -171$ °C).[114] Therefore, the absence of split T_g peaks in $ZnCl_2$−3MeOH and $ZnCl_2$−4MeOH mixtures indicates more homogeneous systems due to a better distribution of $ZnCl_2$ molecules among MeOH molecules, resulting in fewer diversity of microstructures. The heat capacity change (ΔC_p) at the glass transitions can reflect the changes in motional and configurational degrees of freedom as well as the strength of the dominant intermolecular interactions.[11,13] The way the ΔC_p values are obtained in this study is shown in Figure 8A for 1:3 and 1:6 molar ratio mixtures of the $ZnCl_2$−MeOH system, following the literature method.[11,13] The ΔC_p values of 1:3−1:7 molar ratio mixtures are ∼3.0 J $°C^{-1}$ g^{-1}, while those of 1:8 and 1:9 molar ratio mixtures are ∼2.0 J $°C^{-1}$ g^{-1}. This clearly shows the more significant changes in the strength of intermolecular interactions and molecular reorganizations in 1:3−1:7 molar ratio mixtures than those in 1:8 and 1:9 molar ratio mixtures during the transition from the glassy state to supercooled liquids.

CONCLUSIONS

The present study reports the spectral, structural, and thermodynamic properties of a series of $ZnCl_2$−MeOH low-melting mixture solvents (LoMMSs) with $ZnCl_2$ concentrations ranging from 6.7 to 25 mol %. To this aim, FTIR spectroscopy, DFT calculations, and DSC measurements were employed. The analysis of the excess spectra assisted by DFT

calculations and supported by 2D-COS helped us to understand the fundamental structural transformations in mixtures when $ZnCl_2$ is mixed with MeOH. The dissociation of prominent MeOH clusters, represented by MeOH trimer, under the effect of $ZnCl_2$ produces MeOH monomer, MeOH dimer, and H-bond-/coordination bond-driven $ZnCl_2$−3MeOH complex. Here, the other produced species is a special geometry of $ZnCl_2$−3MeOH complex containing largely red-shifted hydroxyls with a significant contribution to the spectral shape. In this scenario, the maximum amount of MeOH monomer and MeOH dimer were found in the $ZnCl_2$−4MeOH mixture, while the maximum amount of $ZnCl_2$−3MeOH complexes was found in the $ZnCl_2$−3MeOH mixture. Moreover, structural and topological studies provided a clear picture of the dissociation process of Zn−Cl bonds when they are solvated by MeOH molecules. Furthermore, the Hirshfeld atomic charges of $ZnCl_2$−MeOH complexes indicated that in each complex, $ZnCl_2$ and MeOH molecules are charged negatively and positively, respectively. This suggests that in the competition between the O/C−H···Cl H-bonds to transfer charge to MeOH and the Zn ← O coordination bond to transfer charge to Zn, the latter always dominates. The thermal behavior and phase transitions of $ZnCl_2$−MeOH mixtures in 1:3−1:9 molar ratios were also investigated by DSC in a temperature range of 20 to −150 °C and a phase diagram was plotted accordingly. The appearance of split T_g peaks suggested the heterogeneity of mixtures and local stoichiometries upon a temperature decrease.

The findings presented in this work on the spectral, structural, topological, and thermodynamic properties of $ZnCl_2$−MeOH mixtures provide useful insights into the underlying microscopic phenomena taking place during the solvation process of salts in alcoholic solutions.

AUTHOR INFORMATION

Corresponding Author

Zhiwu Yu − *MOE Key Laboratory of Bioorganic Phosphorous Chemistry and Chemical Biology, Department of Chemistry, Tsinghua University, Beijing 100084, China;* orcid.org/0000-0002-0192-4796; Phone: (+86) 10 6279 2492; Email: yuzhw@tsinghua.edu.cn; Fax: (+86) 10 6277 1149

Authors

Payam Kalhor − *MOE Key Laboratory of Bioorganic Phosphorous Chemistry and Chemical Biology, Department of Chemistry, Tsinghua University, Beijing 100084, China;*

Institute of Nanotechnology, Karlsruhe Institute of Technology, 76344 Eggenstein-Leopoldshafen, Germany; Institute of Theoretical Informatics, Karlsruhe Institute of Technology, 76131 Karlsruhe, Germany

Zhaoxi Sun − *Changping Laboratory, Beijing 102206, China*

Notes

The authors declare no competing financial interest.

ACKNOWLEDGMENTS

This work was supported by the National Natural Science Foundation of China (No. 22233006).

REFERENCES

(1) Schreckenberg, J. M. A.; Dufal, S.; Haslam, A. J.; Adjiman, C. S.; Jackson, G.; Galindo, A. Modelling of the Thermodynamic and Solvation Properties of Electrolyte Solutions with the Statistical Associating Fluid Theory for Potentials of Variable Range. *Mol. Phys.* **2014**, *112* (17), 2339−2364.

(2) Pinho, S. P.; Macedo, E. A. Solubility of NaCl, NaBr, and KCl in Water, Methanol, Ethanol, and Their Mixed Solvents. *J. Chem. Eng. Data* **2005**, *50*, 29−32.

(3) Li, M.; Constantinescu, D.; Wang, L.; Mohs, A.; Gmehling, J. Solubilities of NaCl, KCl, LiCl, and LiBr in Methanol, Ethanol, Acetone, and Mixed Solvents and Correlation Using the LIQUAC Model. *Ind. Eng. Chem. Res.* **2010**, *49*, 4981−4988.

(4) Long, B.; Zhao, D.; Liu, W. Thermodynamics Studies on the Solubility of Inorganic Salt in Organic Solvents: Application to KI in Organic Solvents and Water-Ethanol Mixtures. *Ind. Eng. Chem. Res.* **2012**, *51*, 9456−9467.

(5) Velez, A. R.; Mufari, J. R.; Rovetto, L. J. Sodium Salts Solubility in Ternary Glycerol + Water + Alcohol Mixtures Present in Purification Process of Crude Glycerol from the Biodiesel Industry. *Fluid Phase Equilib.* **2019**, *497*, 55−63.

(6) Takamuku, T.; Yamamoto, M.; To, T.; Matsugami, M. Solvation Structures of Tetraethylammonium Bromide and Tetrafluoroborate in Aqueous Binary Solvents with Ethanol, Trifluoroethanol, and Acetonitrile. *J. Phys. Chem. B* **2020**, *124*, 5009−5020.

(7) Tan, T. C.; Tan, R.; Soon, L. H.; Ong, S. H. P. Prediction and Experimental Verification of the Effect of Salt on the Vapour-Liquid Equilibrium of Ethanol/1-Propanol/Water Mixture. *Fluid Phase Equilib.* **2005**, *234*, 84−93.

(8) Sardroodi, J. J.; Zafarani-moattar, M. T. Vapor Pressures and Apparent Molal Volumes of the Solutions of $ZnCl_2$ in Ethanol at 298.15 K. *Fluid Phase Equilib.* **2005**, *230*, 64−71.

(9) Tsurko, E. N.; Neueder, R. Conductivity and Association of NaCl, NaBr, NaI, $NaNO_3$, $NaClO_4$ and in Ethanol at 213.15−333.15 K. *Mendeleev Commun.* **2006**, *16*, 334−336.

(10) Lopes, J. M.; Paninho, A. B.; Môlho, M. F.; Nunes, A. V. M.; Rocha, A.; Lourenço, N. M. T.; Najdanovic-visak, V. Biocompatible Choline Based Ionic Salts: Solubility in Short-Chain Alcohols. *J. Chem. Thermodyn.* **2013**, *67*, 99−105.

(11) Terashima, Y.; Sugimoto, N.; Mori, M.; Kinoshita, N.; Takeda, K. Effects of Solvents and Solutes on Glass-Transition Thermodynamics and Kinetic Fragility for Amine and Alcohol Solutions of Inorganic Salts. *J. Therm. Anal. Calorim.* **2019**, *135*, 2797−2805.

(12) Abbott, A. P.; Barron, J. C.; Ryder, K. S.; Wilson, D. Eutectic-Based Ionic Liquids with Metal-Containing Anions and Cations. *Chem. - Eur. J.* **2007**, *13*, 6495−6501, DOI: 10.1002/chem.200601738.

(13) Terashima, Y.; Mori, M.; Takeda, K. Fragility and Glass Transition for Binary Mixtures of 1,2-Propanediamine and $NaClO_4$. *J. Therm. Anal. Calorim.* **2016**, *123*, 1777−1785.

(14) Abbott, A. P.; Alabdullah, S. S. M.; Al-murshedi, A. Y. M.; Ryder, K. S. Brønsted Acidity in Deep Eutectic Solvents and Ionic Liquids. *Faraday Discuss.* **2018**, *206*, 365−377.
(15) Abbott, A. P.; Capper, G.; Davies, D. L.; Rasheed, R. K.; Tambyrajah, V. Novel Solvent Properties of Choline Chloride/Urea Mixtures. *Chem. Commun.* **2003**, 70−71.
(16) Francisco, M.; Van Den Bruinhorst, A.; Kroon, M. C. New Natural and Renewable Low Transition Temperature Mixtures (LTTMs): Screening as Solvents for Lignocellulosic Biomass Processing. *Green Chem.* **2012**, *14*, 2153−2157.
(17) Francisco, M.; van den Bruinhorst, A.; Kroon, M. C. Low-Transition-Temperature Mixtures (LTTMs): A New Generation of Designer Solvents. *Angew. Chem., Int. Ed.* **2013**, *52*, 3074−3085, DOI: 10.1002/anie.201207548.
(18) Chen, Y.; Yu, Z. Low-Melting Mixtures Solvents: Extension of Deep Eutectic Solvents and Ionic Liquids for Broadening Green Solvents and Green Chemistry. *Green Chem. Eng.* DOI: 10.1016/j.gce.2023.11.001.
(19) Kalhor, P.; Ghandi, K. Deep Eutectic Solvents for Pretreatment, Extraction, and Catalysis of Biomass and Food Waste. *Molecules* **2019**, *24*, 4012.
(20) Kalhor, P.; Ghandi, K. Deep Eutectic Solvents as Catalysts for Upgrading Biomass. *Catalysts* **2021**, *11*, 178.
(21) Kalhor, P.; Wang, Y. Q.; Yu, Z. W. The Structures of $ZnCl_2$-Ethanol Mixtures, a Spectroscopic and Quantum Chemical Calculation Study. *Molecules* **2021**, *26*, 2498.
(22) Yu, Q.; Song, Z.; Chen, X.; Fan, J.; Clark, J. H.; Wang, Z.; Sun, Y.; Yuan, Z. A Methanol-Choline Chloride Based Deep Eutectic Solvent Enhances the Catalytic Oxidation of Lignin into Acetovanillone and Acetic Acid. *Green Chem.* **2020**, *22*, 6415−6423.
(23) Abbott, A. P.; Harris, R. C.; Ryder, K. S. Application of Hole Theory to Define Ionic Liquids by Their Transport Properties. *J. Phys. Chem. B* **2007**, *111* (18), 4910−4913.
(24) Bi, W. T.; Tian, M. L.; Row, K. H. Evaluation of Alcohol-Based Deep Eutectic Solvent in Extraction and Determination of Flavonoids with Response Surface Methodology Optimization. *J. Chromatogr. A* **2013**, *1285*, 22−30.
(25) Altunay, N.; Elik, A.; Gürkan, R. Preparation and Application of Alcohol Based Deep Eutectic Solvents for Extraction of Curcumin in Food Samples Prior to Its Spectrophotometric Determination. *Food Chem.* **2020**, *310*, No. 125933.
(26) Rybicki, M.; Hawlicka, E. Solvation of Mg^{2+} Ions in Methanol-Water Mixtures: Molecular Dynamics Simulation. *Chem. Phys.* **2012**, *400*, 79−85.
(27) Anikeenko, A. V.; Zelikman, M. V.; Kadtsyn, E. D.; Medvedev, N. N. Simulationn of Glycyrrhizic Acid Associates with Cholesterol in Methanol. *J. Struct. Chem.* **2017**, *58* (2), 268−275.
(28) Kalhor, P.; Xu, J.; Ashraf, H.; Cao, B. B.; Yu, Z. W. Structural Properties and Hydrogen-Bonding Interactions in Binary Mixtures Containing a Deep-Eutectic Solvent and Acetonitrile. *J. Phys. Chem. B* **2020**, *124*, 1229−1239.
(29) Ashraf, H.; Cao, B. B.; Kalhor, P.; Yu, Z. W. Identification and Properties of Ion-Pairs in the Aqueous Solutions of LiI and NaI by FTIR and Quantum Chemical Calculations. *J. Mol. Liq.* **2021**, *322*, No. 114891.
(30) Kalhor, P.; Ghandi, K.; Ashraf, H.; Yu, Z. W. The Structural Properties of $ZnCl_2$-Ethylene Glycol Binary System and the Peculiarities at the Eutectic Composition. *Phys. Chem. Chem. Phys.* **2021**, *23*, 13136−13147.
(31) Falk, M.; Whalley, E. Infrared Spectra of Methanol and Deuterated Methanols in Gas, Liquid, and Solid Phases. *J. Chem. Phys.* **1961**, *34*, 1554−1568.
(32) Sarkar, S.; Joarder, R. N. Molecular Clusters and Correlations in Liquid Methanol at Room Temperature. *J. Chem. Phys.* **1993**, *99*, 2032−2039.
(33) Yukhnevich, G. V.; Tarakanova, E. G. Hydrogen Bond CH···O in Liquid Methanol. *J. Mol. Struct.* **1998**, *447*, 257−261.
(34) Pagliai, M.; Cardini, G.; Righini, R.; Schettino, V. Hydrogen Bond Dynamics in Liquid Methanol. *J. Chem. Phys.* **2003**, *119*, 6655−6662.
(35) Ohno, K.; Shimoaka, T.; Akai, N.; Katsumoto, Y. Relationship between the Broad OH Stretching Band of Methanol and Hydrogen-Bonding Patterns in the Liquid Phase. *J. Phys. Chem. A* **2008**, *112*, 7342−7348.
(36) Chen, S. D.; Lei, Q. F.; Fang, W. J. Viscosities and Densities for Binary Mixtures of N-Methylpiperazine with Methanol, Ethanol, n-Propanol, Iso-Propanol, n-Butanol and Iso-Butanol at 293.15, 298.15 and 303.15 K. *Fluid Phase Equilib.* **2005**, *234*, 22−33.
(37) Li, Q. Z.; Wu, G. S.; Yu, Z. W. The Role of Methyl Groups in the Formation of Hydrogen Bond in DMSO-Methanol Mixtures. *J. Am. Chem. Soc.* **2006**, *128*, 1438−1439.
(38) Zhang, Q. G.; Wang, N. N.; Wang, S. L.; Yu, Z. W. Hydrogen Bonding Behaviors of Binary Systems Containing the Ionic Liquid 1-Butyl-3-Methylimidazolium Trifluoroacetate and Water/Methanol. *J. Phys. Chem. B* **2011**, *115*, 11127−11136.
(39) Zaitseva, K. V.; Varfolomeev, M. A.; Solomonov, B. N. Thermodynamic Functions of Hydrogen Bonding of Amines in Methanol Derived from Solution Calorimetry Data and Headspace Analysis. *Thermochim. Acta* **2012**, *535*, 8−16.
(40) Alberding, B. G.; Lear, B. J. Concentration-Dependent Dynamics of Hydrogen Bonding between Acetonitrile and Methanol as Determined by 1D Vibrational Spectroscopy. *J. Phys. Chem. A* **2014**, *118*, 4363−4371.
(41) Russina, O.; Mariani, A.; Caminiti, R.; Triolo, A. Structure of a Binary Mixture of Ethylammonium Nitrate and Methanol. *J. Solution Chem.* **2015**, *44*, 669−685.
(42) Mariani, A.; Russina, O.; Caminiti, R.; Triolo, A. Structural Organization in a Methanol:Ethylammonium Nitrate (1:4) Mixture: A Joint X-Ray/Neutron Diffraction and Computational Study. *J. Mol. Liq.* **2015**, *212*, 947−956.
(43) Sulaiman, M. I.; Yang, S.; Ellis, A. M. Infrared Spectroscopy of Methanol and Methanol/Water Clusters in Helium Nanodroplets: The OH Stretching Region. *J. Phys. Chem. A* **2017**, *121*, 771−776.
(44) Kim, K. S.; Park, B. H. Volumetric Properties of Solutions of Choline Chloride + Glycerol Deep Eutectic Solvent with Water, Methanol, Ethanol, or Iso-Propanol. *J. Mol. Liq.* **2018**, *254*, 272−279.
(45) Han, Y. F.; Liu, R. R.; Jiang, C. Y.; Wang, H. G.; Zheng, X. M. The Aggregation Structure of a Methanol/$CHCl_3$ Binary Mixture Investigated by Polarized Raman Spectroscopy and HNMR. *J. Mol. Liq.* **2021**, *335*, No. 116224.
(46) Safarov, J. T. Vapor Pressure of Heat Transfer Fluids of Absorption Refrigeration Machines and Heat Pumps: Binary Solutions of Lithium Nitrate with Methanol. *J. Chem. Thermodyn.* **2005**, *37*, 1261−1267.
(47) Safarov, J. T. Investigation of the Vapor Pressure p of Zinc Bromide or Zinc Chloride Solutions with Methanol by Static Method. *J. Chem. Thermodyn.* **2006**, *38*, 304−311.
(48) Megyes, T.; Balint, S.; Bako, I.; Grosz, T.; Radnai, T.; Palinkas, G. Solvation of Calcium Ion in Methanol: Comparison of Diffraction Studies and Molecular Dynamics Simulation. *Chem. Phys.* **2006**, *327*, 415−426.
(49) Yu, X. C.; Lin, K.; Hu, N. Y.; Zhou, X. G.; Liu, S. L. Effects of Salts on the Microstructure of Methanol. *Acta Phys. Chim. Sin.* **2010**, *26*, 2473−2480.
(50) Singh, D. K.; Mishra, S.; Ojha, A. K.; Srivastava, S. K.; Schluecker, S.; Asthana, B. P.; Popp, J.; Singh, R. K. Hydrogen Bonding in Different Pyrimidine-Methanol Clusters Probed by Polarized Raman Spectroscopy and DFT Calculations. *J. Raman Spectrosc.* **2011**, *42* (4), 667−675.
(51) Zeng, L. M.; Li, Z. B.; Wang, X. L. Determination and Modeling of $MgCl_2$ Solubility in Methanol, Ethanol, 2-Propanol, and Their Mixtures from 283 to 343 K. *J. Chem. Eng. Data* **2016**, *61*, 797−805.
(52) Iyoki, S.; Takigawa, T.; Uemura, T. Thermal and Physical Properties of the Methanol-Lithium Bromide-Zinc Chloride System. *Int. J. Refrig.* **1991**, *14*, 78−85.

(53) Wang, W. T.; Zhang, J.; Jiang, F.; Wang, X. H.; Wang, Z. G. Reprocessable Supramolecular Thermoplastic BAB-Type Triblock Copolymer Elastomers with Enhanced Tensile Strength and Toughness via Metal − Ligand Coordination. *ACS Appl. Polym. Mater.* **2019**, *1*, 571−583.
(54) Du, H. R.; Qi, X. Q.; Qie, L.; Huang, Y. H. A Nonflammable Organic Electrolyte with a Weak Association State for Zinc Batteries Operated at - 78.5 °C. *Adv. Funct. Mater.* **2023**, *33*, No. 2302546.
(55) Soriano, N. U.; Venditti, R.; Argyropoulos, D. S. Biodiesel Synthesis via Homogeneous Lewis Acid-Catalyzed Transesterification. *Fuel* **2009**, *88*, 560−565, DOI: 10.1016/j.fuel.2008.10.013.
(56) Amani, V.; Ahmadi, R.; Naseh, M.; Ebadi, A. Synthesis, Spectroscopic Characterization, Crystal Structure and Thermal Analyses of Two Zinc (II) Complexes with Methanolysis of 2-pyridinecarbonitrile as a Chelating Ligand. *J. Iran. Chem. Soc.* **2017**, *14* (3), 635−642.
(57) Li, Q. Z.; Wang, N. N.; Zhou, Q.; Sun, S. Q.; Yu, Z. W. Excess Infrared Absorption Spectroscopy and Its Applications in the Studies of Hydrogen Bonds in Alcohol-Containing Binary Mixtures. *Appl. Spectrosc.* **2008**, *62*, 166−170.
(58) Wallace, V. M.; Dhumal, N. R.; Zehentbauer, F. M.; Kim, H. J.; Kiefer, J. Revisiting the Aqueous Solutions of Dimethyl Sulfoxide by Spectroscopy in the Mid- and near-Infrared: Experiments and Car-Parrinello Simulations. *J. Phys. Chem. B* **2015**, *119*, 14780−14789.
(59) Kalhor, P.; Yu, Z. W. Structural and Hydrogen-Bonding Properties of Neat t-BuNH_2 and Its Binary Mixtures with CCl_4, $CHCl_3$ and DMSO. *J. Mol. Struct.* **2020**, *1215*, No. 128257.
(60) Noda, I. Two-Dimensional Infrared (2D IR) Spectroscopy: Theory and Applications. *Appl. Spectrosc.* **1990**, *44*, 550−561.
(61) Hansen, W. N. Expanded Formulas for Attenuated Total Reflection and the Derivation of Absorption Rules for Single and Multiple ATR Spectrometer Cells. *Spectrochim. Acta* **1965**, *21*, 815−833.
(62) Zhou, Y.; Xu, J.; Wang, N. N.; Yu, Z. W. Excess Spectroscopy: Concept and Applications. *Acta Phys. -Chim. Sin.* **2016**, *32*, 239−248.
(63) Zhang, Y. Q.; Wu, Z. W.; Wang, Y. Q.; He, H. Y.; Yu, Z. W. Excess Spectroscopy and Its Applications in the Study of Solution Chemistry. *Pure Appl. Chem.* **2020**, *92*, 1611−1626.
(64) Wang, N. N.; Li, Q. Z.; Yu, Z. W. Hydrogen Bonding Interactions in Three 2-Mercaptoethanol Systems: An Excess Infrared Spectroscopic Study. *Appl. Spectrosc.* **2009**, *63*, 1356−1362.
(65) Kalhor, P.; Li, Q. Z.; Zheng, Y. Z.; Yu, Z. W. Is the Fourier Transform Infrared Free-OH Band of t-Butanol Only from Free OHs? Case Studies on the Binary Systems of the Alcohol with CCl_4 and $CHCl_3$. *J. Phys. Chem. A* **2020**, *124*, 6177−6185.
(66) Yu, Z. W.; Noda, I. On the Normalization Method in Two-Dimensional Correlation Spectra When Concentration Is Used as a Perturbation Parameter. *Appl. Spectrosc.* **2003**, *57*, 164−167.
(67) Frisch, M. J.; Trucks, G. W.; Schlegel, H. B.; Scuseria, G. E.; Robb, M. A.; Cheeseman, J. R.; Scalmani, G.; Barone, V.; Mennucci, B.; Petersson, G. A.et al. *Gaussian 09*, Revision D.01; Gaussian Inc.: Wallingford, CT, 2009.
(68) Wang, L.; Ishiyama, T.; Morita, A. Theoretical Investigation of C-H Vibrational Spectroscopy. 2. Unified Assignment Method of IR, Raman, and Sum Frequency Generation Spectra of Ethanol. *J. Phys. Chem. A* **2017**, *121*, 6701−6712.
(69) Malloum, A.; Fifen, J. J.; Conradie, J. Solvation Energies of the Proton in Methanol Revisited and Temperature Effects. *Phys. Chem. Chem. Phys.* **2018**, *20*, 29184−29206.
(70) Kalhor, P.; Zheng, Y. Z.; Ashraf, H.; Cao, B. B.; Yu, Z. W. Influence of Hydration on the Structure and Interactions of Ethaline Deep-Eutectic Solvent: A Spectroscopic and Computational Study. *ChemPhysChem* **2020**, *21*, 995−1005.
(71) Tlili, M.; Abdelmoulahi, H.; Trabelsi, S.; Nasr, S.; González, M. A.; Cuello, G. J.; Bellissent-funel, M.; Darpentigny, J. Hydrogen-Bond Network in Liquid Methanol as Studied by Neutron Scattering, DFT Calculations and Molecular Dynamics Simulations. *J. Mol. Struct.* **2021**, *1227*, No. 129683.
(72) Barone, V.; Cossi, M. Quantum Calculation of Molecular Energies and Energy Gradients in Solution by a Conductor Solvent Model. *J. Phys. Chem. A* **1998**, *102*, 1995−2001.
(73) Boys, S. F.; Bernardi, F. The Calculation of Small Molecular Interactions by the Differences of Separate Total Energies. Some Procedures with Reduced Errors. *Mol. Phys.* **1970**, *19*, 553−566.
(74) Hirshfeld, F. L. Bonded-Atom Fragments for Describing Molecular Charge Densities. *Theor. Claim. Acta* **1977**, *44*, 129−138.
(75) Bader, R. F. W. *Atoms in Molecules: A Quantum Theory*; Oxford, 1990.
(76) Lu, T.; Chen, F. W. Multiwfn: A Multifunctional Wavefunction Analyzer. *J. Comput. Chem.* **2012**, *33* (5), 580−592.
(77) Hagen, W.; Tielens, A.; Greenberg, J. M. The Three Micron "Ice" Band in Grain Mantles. *Astron. Astrophys. Suppl. Ser.* **1983**, *51*, 389−416.
(78) Hänninen, V.; Halonen, L. Calculation of Spectroscopic Parameters and Vibrational Overtones of Methanol. *Mol. Phys.* **2003**, *101*, 2907−2916.
(79) Joseph, J.; Jemmis, E. D. Red-, Blue-, or No-Shift in Hydrogen Bonds: A Unified Explanation. *J. Am. Chem. Soc.* **2007**, *129*, 4620−4632.
(80) Chen, Y.; Yu, D. K.; Chen, W. J.; Fu, L.; Mu, T. C. Water Absorption by Deep Eutectic Solvents. *Phys. Chem. Chem. Phys.* **2019**, *21*, 2601−2610.
(81) Beck, J. P.; Cimas, A.; Lisy, J. M.; Gaigeot, M. P. O−H Anharmonic Vibrational Motions in $Cl^-\cdots(CH_3OH)_{1-2}$ Ionic Clusters. Combined IRPD Experiments and AIMD Simulations. *Spectrochim. Acta, Part A* **2014**, *119*, 12−17.
(82) Kiefer, J.; Molina, M. M.; Noack, K. The Peculiar Nature of Molecular Interactions between an Imidazolium Ionic Liquid and Acetone. *ChemPhysChem* **2012**, *13*, 1213−1220.
(83) Xu, J.; Deng, G.; Wang, Y. T.; Guo, H. Y.; Kalhor, P.; Yu, Z. W. Local Acid Strength of Solutions and Its Quantitative Evaluation Using Excess Infrared Nitrile Probes. *J. Phys. Chem. Lett.* **2020**, *11*, 1007−1012.
(84) Zhou, Y.; Zheng, Y. Z.; Sun, H. Y.; Deng, G.; Yu, Z. W. Two-State or Non-Two-State? An Excess Spectroscopy-Based Approach to Differentiate the Existing Forms of Molecules in Liquids Mixtures. *Sci. Rep.* **2015**, *5*, No. 16379, DOI: 10.1038/srep16379.
(85) Pauling, L. *The Nature of the Chemical Bond*, 3rd ed.; Cornell University Press: New York, 1960.
(86) Bondi, A. Van Der Waals Volumes and Radii. *J. Phys. Chem. A* **1964**, *68*, 441−451.
(87) Cordero, B.; Gomez, V.; Platero-Prats, A. E.; Reves, M.; Echeverria, J.; Cremades, E.; Barragan, F.; Alvarez, S. Covalent Radii Revisited. *Dalt. Trans.* **2008**, 2832−2838.
(88) Tanaka, Y.; Ohtorno, N.; Arakawa, K. The Structure of Liquid Alcohols by Neutron and X-Ray Diffraction. III. Liquid Structure of Methanol. *Bull. Chern. Soc. Jpn.* **1985**, *58*, 270−276, DOI: 10.1246/BCSJ.58.270.
(89) Wagle, D. V.; Deakyne, C. A.; Baker, G. A. Quantum Chemical Insight into the Interactions and Thermodynamics Present in Choline Chloride Based Deep Eutectic Solvents. *J. Phys. Chem. B* **2016**, *120*, 6739−6746.
(90) Garcia, G.; Atilhan, M.; Aparicio, S. An Approach for the Rationalization of Melting Temperature for Deep Eutectic Solvents from DFT. *Chem. Phys. Lett.* **2015**, *634*, 151−155.
(91) Stefanovic, R.; Ludwig, M.; Webber, G. B.; Atkin, R.; Page, A. J. Nanostructure, Hydrogen Bonding and Rheology in Choline Chloride Deep Eutectic Solvents as a Function of the Hydrogen Bond Donor. *Phys. Chem. Chem. Phys.* **2017**, *19*, 3297−3306.
(92) Faraone, A.; Wagle, D. V.; Baker, G. A.; Novak, E. C.; Ohl, M.; Reuter, D.; Lunkenheimer, P.; Loidl, A.; Mamontov, E. Glycerol Hydrogen-Bonding Network Dominates Structure and Collective Dynamics in a Deep Eutectic Solvent. *J. Phys. Chem. B* **2018**, *122* (3), 1261−1267.
(93) Jablonski, M. Study of Beryllium, Magnesium, and Spodium Bonds to Carbenes and Carbodiphosphoranes. *Molecules* **2021**, *26*, 2275.

(94) Yáñez, M.; Sanz, P.; Mó, O.; Alkorta, I.; Elguero, J. Beryllium Bonds, Do They Exist? *J. Chem. Theory Comput.* **2009**, *5*, 2763−2771.
(95) Martín-sómer, A.; Lamsabhi, A. M.; Mó, O.; Yáñez, M. The Importance of Deformation on the Strength of Beryllium Bonds. *Comput. Theor. Chem.* **2012**, *998*, 74−79.
(96) Alkorta, I.; Legon, A. C. Non-Covalent Interactions Involving Alkaline-Earth Atoms and Lewis Bases B: An Ab Initio Investigation of Beryllium and Magnesium Bonds, B··· MR2 (M = Be or Mg and R = H, F or CH_3). *Inorganics* **2019**, *7*, 35.
(97) Espinosa, E.; Alkorta, I.; Elguero, J.; Molins, E. From Weak to Strong Interactions: A Comprehensive Analysis of the Topological and Energetic Properties of the Electron Density Distribution Involving Systems. *J. Chem. Phys.* **2002**, *117*, 5529−5542.
(98) Lu, T.; Chen, F. W. Bond Order Analysis Based on the Laplacian of Electron Density in Fuzzy Overlap Space. *J. Phys. Chem. A* **2013**, *117*, 3100−3108.
(99) Becke, A. D.; Edgecombe, K. E. A Simple Measure of Electron Localization in Atomic and Molecular Systems. *J. Chern. Phys.* **1990**, *92*, 5397−5403.
(100) Magini, M.; Paschina, G.; Piccaluga, G. On the Structure of Methyl Alcohol at Room Temperature. *J. Chem. Phys.* **1982**, *77*, 2051−2056.
(101) Zheng, Y. Z.; Wang, N. N.; Luo, J. J.; Zhou, Y.; Yu, Z. W. Hydrogen-Bonding Interactions between [BMIM][BF_4] and Acetonitrile. *Phys. Chem. Chem. Phys.* **2013**, *15*, 18055−18064.
(102) Jorgensen, W. L. Quantum and Statistical Mechanical Studies of Liquids. 7. Structure and Properties of Liquid Methanol. *J. Am. Chem. Soc.* **1980**, *102*, 543−549.
(103) Ihmels, E. C.; Safarov, J. T. (P, ρ,T) Properties and Apparent Molar Volumes Vφ of $ZnCl_2$ in CH_3OH. *J. Chem. Eng. Data* **2006**, *51*, 1015−1019.
(104) Dupont, N.; Grenouillet, P.; Bornette, F.; de Bellefon, C. Switching from Water to Ionic Liquids for the Production of Methylchloride: Catalysis and Reactor Issues. *Chem. Eng. J.* **2009**, *145*, 441−445, DOI: 10.1016/j.cej.2008.04.031.
(105) Shaabani, A.; Keshipour, S.; Shaabani, S.; Mahyari, M. Zinc Chloride Catalyzed Three-Component Ugi Reaction: Synthesis of N-Cyclohexyl-2-(2hydroxyphenylamino) Acetamide Derivatives. *Tetrahedron Lett.* **2012**, *53*, 1641−1644.
(106) Aysu, T.; Kucuk, M. M. Liquefaction of Giant Fennel (Ferula Orientalis L.) in Supercritical Organic Solvents: Effects of Liquefaction Parameters on Product Yields and Character. *J. Supercrit. Fluids* **2013**, *83*, 104−123.
(107) Aysu, T.; Durak, H. Bio-Oil Production via Catalytic Supercritical Liquefaction of Syrian Mesquite (Prosopis Farcta). *J. Supercrit. Fluids* **2016**, *109*, 26−34.
(108) Jangir, L. K.; Kumari, Y.; Kumar, A.; Kumar, M.; Awasthi, K. Investigation of Luminescence and Structural Properties of ZnO Nanoparticles, Synthesized with Different Precursors. *Mater. Chem. Front.* **2017**, *1*, 1413−1421, DOI: 10.1039/C7QM00058H.
(109) Knorr, A.; Stange, P.; Fumino, K.; Weinhold, F.; Ludwig, R. Spectroscopic Evidence for Clusters of Like-Charged Ions in Ionic Liquids Stabilized by Cooperative Hydrogen Bonding. *ChemPhysChem* **2016**, *17*, 458−462.
(110) Hussin, S. A. M.; Varanusupakul, P.; Shahabuddin, S.; Hui, B. Y.; Mohamad, S. Synthesis and Characterization of Green Menthol-Based Low Transition Temperature Mixture with Tunable Thermophysical Properties as Hydrophobic Low Viscosity Solvent. *J. Mol. Liq.* **2020**, *308*, No. 113015, DOI: 10.1016/j.molliq.2020.113015.
(111) Martos, M.; Pastor, I. M. Imidazolium-Urea Low Transition Temperature Mixtures for the UHP-Promoted Oxidation of Boron Compounds. *J. Mol. Liq.* **2022**, *347*, No. 118349.
(112) Hall, C. L.; Potticary, J.; Hamilton, V.; Gaisford, S.; Buanz, A.; Hall, S. R. Metastable Crystalline Phase Formation in Deep Eutectic Systems Revealed by Simultaneous Synchrotron XRD and DSC. *Chem. Commun.* **2020**, *56*, 10726−10729.
(113) Kanno, H.; Yamauchi, S. Raman Spectral Changes of Alcoholic Zinc Chloride Solutions from Liquid State to Glassy State. *J. Solution Chem.* **1991**, *20*, 589−594.
(114) Sugisaki, M.; Suga, H.; Seki, S. Finding of the Glass-Transition Phenomena of Methanol. *Bull. Chem. Soc. Jpn.* **1967**, *40*, 2984.